Available online at www.sciencedirect.com
ScienceDirect
Journal of Crystal Growth 310 (2008) 2339–2344
JOURNAL OF CRYSTAL GROWTH
www.elsevier.com/locate/jcrysgro

In situ stress measurement for MOVPE growth of high efficiency lattice-mismatched solar cells

J.F. Geisz*, A.X. Levander[1], A.G. Norman, K.M. Jones, M.J. Romero

National Renewable Energy Laboratory, 1617 Cole Blvd., Golden, CO 80401 USA

Available online 19 November 2007

Abstract

We have recently reported high efficiencies in a monolithic III–V triple-junction solar cell design that is grown inverted with a metamorphic 1.0 eV bottom $In_{.27}Ga_{.73}As$ junction. The biaxial stress and strain grown into this highly lattice-mismatched junction can be controlled by varying the design of a step-graded $Ga_xIn_{1-x}P$ buffer layer, in which most, but not all, of the 1.9% misfit strain is relieved. A multi-beam optical stress sensor (MOSS) is a convenient tool for *in situ* measurement of stress during metal–organic vapor phase epitaxy (MOVPE) for the optimization of solar cell performance. The analysis of stress from curvature data is complicated by significant temperature effects due to relatively small thermal gradients in our atmospheric-pressure MOVPE reactor. These temperature effects are discussed and approximations made to allow practical analysis of the data. The results show excellent performance of inverted $In_{.27}Ga_{.73}As$ solar cells grown with slight compressive stress, but degradation under tensile stress. The best devices had a V_{oc} of 0.54 V and a dislocation density in the low $10^6\,cm^{-2}$. The *in situ* stress data is also compared with *ex situ* strain data derived from X-ray diffraction measurements.
© 2007 Published by Elsevier B.V.

PACS: 81.15.Gh; 61.72.Uj; 61.72.Ff; 62.40.+i

Keywords: A1. Stresses; A3. Organometallic vapor phase epitaxy; B2. Semiconducting III–V materials; B3. Solar Cells

1. Introduction

The ability to use lattice-mismatched III–V semiconductor alloys in opto-electronic devices such as solar cells greatly expands the potential for increased performance. We have recently demonstrated record breaking efficiencies in a monolithic III–V triple-junction solar cell design that utilizes a lattice mismatched 1.0 eV $In_{.27}Ga_{.73}As$ bottom junction [1]. This triple-junction design is grown inverted, so that traditional $Ga_{.5}In_{.5}P$ and GaAs top junctions are lattice matched to the GaAs substrate. The excellent performance of this lattice-mismatched bottom junction is a result of relatively low defect densities in the active junction by growing a compositionally step-graded GaInP buffer. The design of this graded buffer has previously been described for another material system [2]. One advantage of this graded buffer design is the ability to grow the active junction with little or no strain, despite incomplete strain relaxation of the buffer layers themselves. Layers grown with low strain are predicted to result in much lower dislocation densities [3].

While the extent of the incomplete relaxation of the buffer layers, which is essential for engineering strain-free active junctions, is difficult to predict, the strain of buffer and active regions has previously been characterized with *ex situ* X-ray diffraction [2]. Multi-beam optical stress sensor (MOSS) is an *in situ* technique that can be used to determine the evolution of film stress from real-time curvature measurements [4]. In this paper, we describe the practical application of MOSS for rapid optimization of layer stresses in the metamorphic solar cell device described above.

*Corresponding author. Tel.: +1 303 384 6474; fax: +1 303 384 6531.
E-mail address: john_geisz@nrel.gov (J.F. Geisz).
[1]Currently at Pennsylvania State University.

0022-0248/$ - see front matter © 2007 Published by Elsevier B.V.
doi:10.1016/j.jcrysgro.2007.11.048

2. Experimental procedure

Lattice-mismatched 1.0 eV $In_{.27}Ga_{.73}As$ single-junction solar cells similar to those used in the multi-junction devices of Ref. [1] were grown by metal–organic vapor phase epitaxy (MOVPE) on (0 0 1) GaAs substrates miscut 2° toward the (1 1 1)B direction. The Si-doped substrates were approximately 350 μm thick. The vertical-tube MOVPE reactor operated at atmospheric pressure (~620 Torr in Golden) without any substrate rotation at a total flow rate of approximately 6 standard liters per minute. The substrate was heated on an inductively heated graphite susceptor. Arsine, phosphine, trimethylgallium, and trimethylindium were used as III–V precursors while hydrogen selenide, disilane, and diethylzinc were used as dopant gases.

The n-on-p $In_{.27}Ga_{.73}As$ homojunction solar cell was grown in an inverted configuration with $In_{.27}Ga_{.73}P$ window and back-surface-field layers as shown schematically in Fig. 1. The entire active device was 1.9% lattice mismatched with the GaAs substrate. The device was grown metamorphically using a compositionally step-graded $Ga_xIn_{1-x}P$ buffer layer similar to that described in Ref. [2]. The grade consisted of eight 0.25 μm-thick steps and a final 1.0 μm-thick $Ga_xIn_{1-x}P$ step that were linearly graded in composition and, therefore, nominal lattice constant. The composition of the final 1.0 μm-thick $Ga_xIn_{1-x}P$ layer was varied from $0.19<x<0.26$ thereby varying the stress and strain in the active $In_{.27}Ga_{.73}As$ solar cell. The active $In_{.27}Ga_{.73}As$ device was grown at 650 °C while the Si-doped step-graded buffer was grown at 620 °C.

A k-space Associates MOSS apparatus was mounted above the MOVPE reactor for *in situ* curvature measurements. The MOSS apparatus split a single 662 nm laser beam into an array of nine parallel beams incident on the sample through a quartz window. The reflected beams were imaged by a charge-coupled device (CCD) camera and analyzed as described elsewhere to determine the change in curvature [4]. The 2-dimensional array of beams allowed curvature in two orthogonal directions to be measured simultaneously. The reference curvature was calibrated to be zero at the beginning of each growth run at room temperature. The film stress during the growth of certain layers was calculated from the curvature measurement as described in the next section.

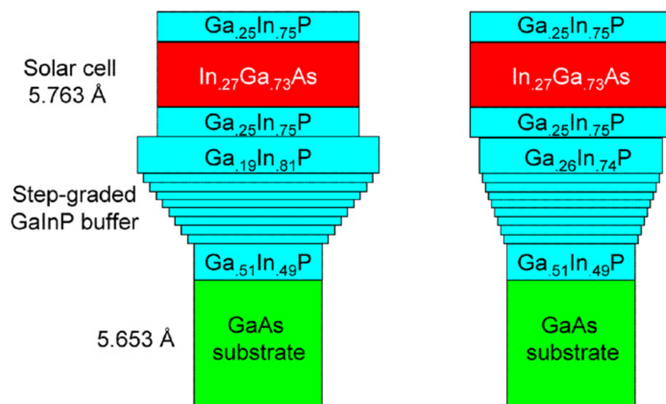

Fig. 1. Schematics of single-junction inverted $In_{.27}Ga_{.73}As$ devices grown for this study illustrating the step-graded GaInP buffer. The width of the layers indicates the nominal lattice constant. Two schematics illustrate the range of grades used. Not to scale.

X-ray diffraction reciprocal space maps (RSM) of the 224 grazing incidence (GI) reflection were measured on a Bede D1 diffractometer. Rather than using a triple-crystal configuration, two 0.5 mm slits were sufficient because of the broadness of the peaks. Two 224GI RSMs were obtained for each sample with the 2° miscut direction aligned perpendicular to the plane of diffraction. The sample was rotated 180° around the axis normal to its surface to obtain the second 224GI RSM. The resulting peak locations were averaged in order to remove the well-known effects of epilayer tilt in this type of metamorphic structure [5]. The results were quantitatively analyzed using the method of van der Sluis [6].

The inverted devices were processed as described in Ref. [1]. Basically, the metamorphic device was mounted on a silicon substrate with a low viscosity epoxy and the GaAs substrate removed. Eleven 0.1 cm^2 devices were defined from each sample with gold grids designed for concentrator measurements using standard photolithographic techniques. Current–voltage measurements were performed on the devices using the air-mass 1.5 direct spectrum (low aerosol optical depth [7]). No antireflective coating was applied. The device band gap (E_g) was determined from quantum efficiency measurements.

Cathodoluminescence (CL) spectrum imaging and transmission electron microscopy (TEM) observations were performed on a few representative devices to characterize defect densities. CL was measured using a 30 keV beam to penetrate past the graded buffer, which acts as a window to the luminescence excited in the InGaAs. TEM analysis was performed on thin cross-section samples prepared in an FEI Nova 200 dual-beam focused-ion-beam workstation and examined in a Philips CM30 TEM operated at 300 kV. The defect structure in the samples was imaged using 220 dark field two-beam diffraction conditions.

2.1. Temperature effects on MOSS analysis

The curvature, κ^0, of a simple two layer structure with a thin-film stress, σ_f, at isothermal temperature, T^0, can be calculated using Stoney's equation [8]:

$$\kappa^0 = -\frac{6\sigma_f^0 h_f}{Y_s h_s^2}, \tag{1}$$

where h_f is the thickness of a deposited thin film, h_s is the thickness of the substrate, and Y_s is the biaxial modulus of the substrate.

Most previous reports of MOSS for *in situ* stress measurement were performed at constant growth temperatures under high-vacuum conditions, resulting in near-isothermal

conditions. Growth of complicated structures, such as multi-junction solar cell devices, often requires changing growth temperatures. While we would prefer to determine the stress with reference to a standard temperature, T_0, any difference in temperature during measurement, T, results in a change of curvature due to a difference in the thermal expansion of the two layers [9]:

$$\kappa^{\mathrm{TE}} = -\frac{6h_{\mathrm{f}}}{Y_{\mathrm{s}}h_{\mathrm{s}}^2} Y_{\mathrm{f}}(\alpha_s - \alpha_{\mathrm{f}})(T - T_0), \tag{2}$$

where Y_{f} is the biaxial modulus of the thin film, α_{s} is the coefficient of thermal expansion of the substrate, and α_{f} is the coefficient of thermal expansion of the thin film.

The high pressures in our atmospheric-pressure MOVPE reactor result in convective cooling of the growing surface and, therefore, a thermal gradient along the thickness of the semiconductor structure. This thermal gradient causes a significant change in curvature even for single-layer substrates [9]:

$$\kappa^{\mathrm{TG}} = \frac{\alpha_{\mathrm{s}}}{h_{\mathrm{s}}}(T_{\mathrm{B}} - T_{\mathrm{U}}), \tag{3}$$

where T_{B} is the temperature of the heated bottom of the sample, and T_{U} is the temperature of the cooled upper surface of the sample. Since the thermal gradient is dominated by the thicker substrate unless the thermal conductivity of the thin film is dramatically different, we assume that this contribution to curvature is primarily a function of substrate properties and the gas flow geometry that determines the convective heat flux. This assumption may also be false if the heat flux is dominated by radiative cooling which would be dependent on the emissivity of the surface layer. In any event, we assume that κ^{TG} is primarily a function of the growth temperature and the substrate properties for a given reactor with constant pressure and flow rates. We have measured this contribution to the curvature in our reactor by annealing a variety of substrate materials and thickness, shown in Fig. 2. We find that the curvature is indeed a strong function of the temperature and material properties, but not of the substrate thickness. We have fit this data to a cubic function:

$$\kappa^{\mathrm{TG}} = B_{\mathrm{s}}T^2(1 + C_{\mathrm{s}}T), \tag{4}$$

where B_{s} and C_{s} are empirical parameters that are dependent on the substrate material.

The measured curvature is therefore the sum of all these contributions:

$$\kappa = \kappa^0 + \kappa^{\mathrm{TE}} + \kappa^{\mathrm{TG}}. \tag{5}$$

Because of the complications of calculating Eq. (2) for real materials and structures, we typically choose the standard temperature to be the growth temperature rather than room temperature, so that $\kappa^{\mathrm{TE}} = 0$. Both h_{f} and σ_{f} vary with time as the film grows and relaxes, but we can calculate an incremental stress at growth temperature from

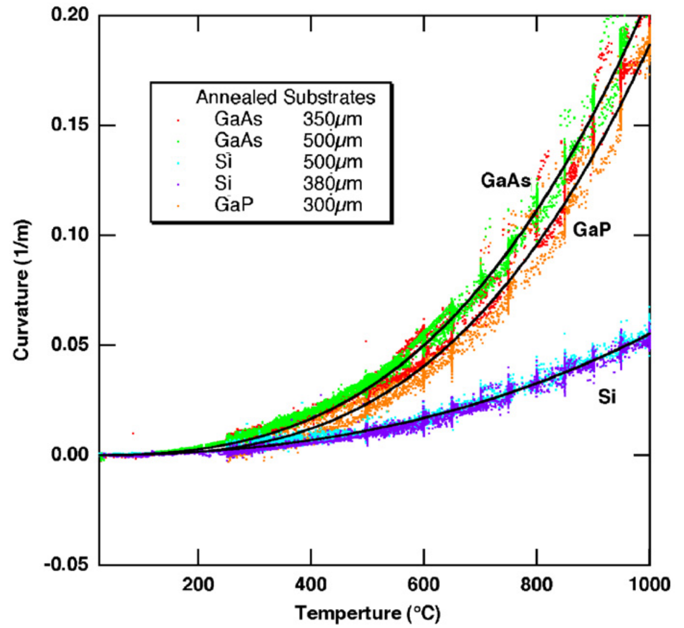

Fig. 2. Curvature of annealed substrates for calibration of thermal gradient effects. Black lines are the fits to Eq. (4) for each substrate material.

the slope of the stress-thickness versus thickness [4]:

$$\sigma_{\mathrm{inc}} = \frac{\mathrm{d}(\sigma_{\mathrm{f}}h_{\mathrm{f}})}{\mathrm{d}h_{\mathrm{f}}} = \frac{Y_{\mathrm{s}}h_{\mathrm{s}}^2}{6\mathrm{GR}}\frac{\mathrm{d}(\kappa - \kappa^{\mathrm{TG}})}{\mathrm{d}t}, \tag{6}$$

where $\mathrm{GR} = \mathrm{d}h_{\mathrm{f}}/\mathrm{d}t$ is the growth rate. If this slope is constant during a growth layer and other layers are not simultaneously relaxing, it is likely that this incremental stress is the layer stress at growth temperature. Note that $\mathrm{d}\kappa^{\mathrm{TG}}/\mathrm{d}t = 0$ within layers of constant growth temperature (based on the assumptions of Eq. (4)), so the resulting stress does not actually depend on the thermal gradient calibration.

3. Results

Fig. 3 shows the real-time measured curvature in two orthogonal directions, κ_x and κ_y, as well as the measured temperature of the susceptor of a typical growth run. The κ^{TG} is calculated from Eq. (4) and shows good agreement with the measured curvature until mismatched layers are grown. From this data, it is clear that the effect of the thermal gradient is similar in magnitude to that of the lattice-mismatched induced stress. Using Eq. (3), we estimate that the temperature difference from front to back of the substrate is less than ~10 °C when the temperature is at 900 °C. The nominal growth rate is also shown on the figure based on previous calibrations, but the growth rate could also be measured from interference oscillations of reflectance data. From these measurements, the data is replotted in Fig. 4 as stress-times-thickness as a function of cumulative thickness. This figure also shows the intended misfit of the layers grown. We can see that during the growth of the first couple mismatched layers of the compositionally step-graded GaInP buffer, compressive

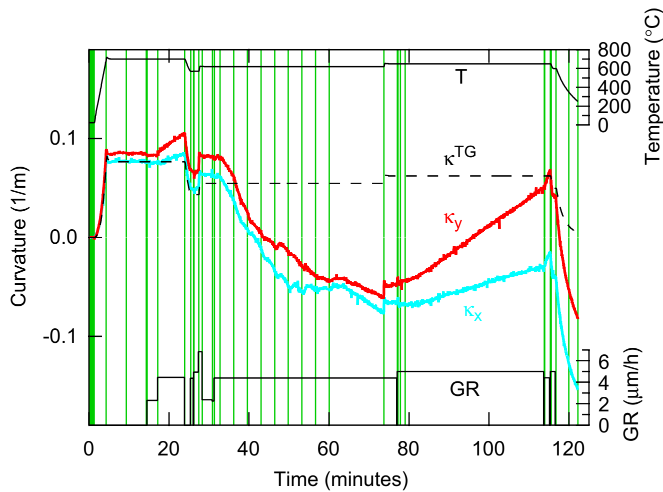

Fig. 3. *In situ* measurements of curvature and temperature during growth of a typical device. The growth rate and κ_{TE} are estimated based on previous calibrations. Vertical lines indicate abrupt changes in growth conditions.

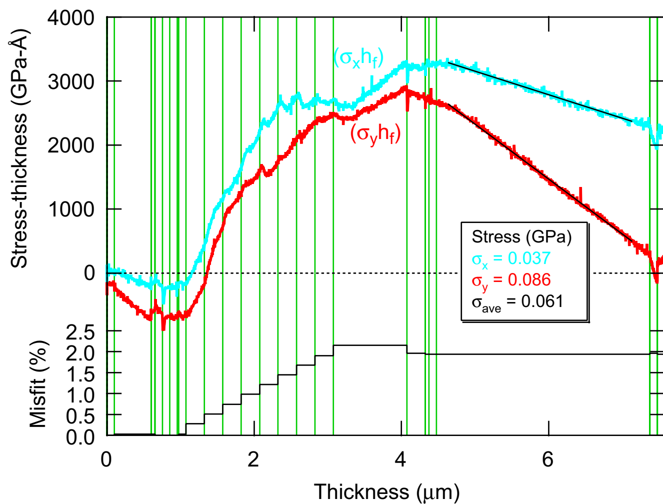

Fig. 4. Stress-times-thickness as a function of cumulative thickness re-plotted from data in Fig. 3. Misfit of nominal material lattice constant with the substrate is also plotted. Vertical lines indicate layer boundaries. Active junction stress is calculated using Eq. (6) from the fit slope.

stress builds with a positive slope. But in subsequent steps, the stress is observed to relax, slowly from reduced slopes or quickly during regions of negative slope within a layer of constant misfit. After much relaxation during the graded buffer, the final thick layer of the $Ga_xIn_{1-x}P$ buffer retains some compressive stress. The negative slope in Fig. 4 indicates tensile stress in the active junction of this buffer composition. The stress in the two orthogonal directions is calculated from Eq. (6) and averaged for subsequent analysis.

Before processing each sample as a device, they were characterized by X-ray diffraction as described above. An example of a 224GI RSM is shown in Fig. 5. From these X-ray measurements, the strained lattice constants of the

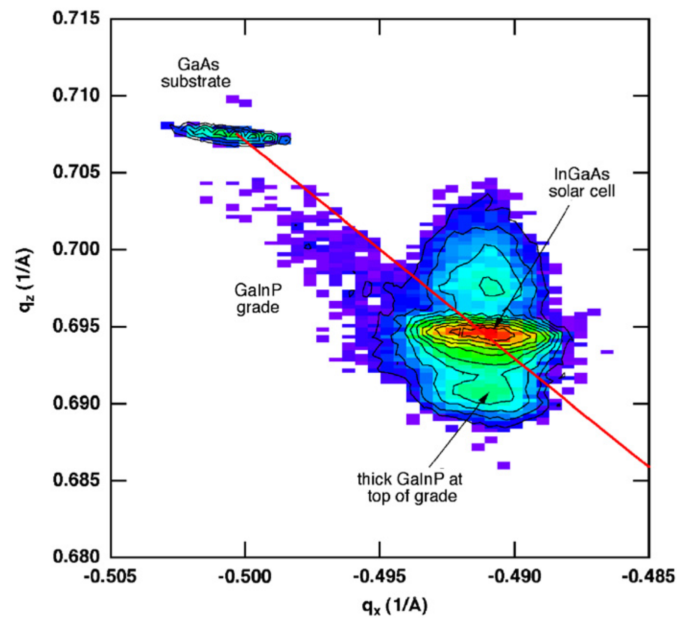

Fig. 5. X-ray diffraction data of typical structure. 224GI RSM. The long (red) line indicates zero strain.

$In_{.27}Ga_{.73}As$ active junction and the thick $Ga_xIn_{1-x}P$ layer at the top of the graded buffer were extracted and, from these, the composition and room temperature strain were calculated. For some compositions of the buffer layer, the $Ga_xIn_{1-x}P$ peak could not be differentiated from the $In_{.27}Ga_{.73}As$ peak, so the nominal rather than the measured composition was used in these cases.

A series of identical 1.0 eV $In_{.27}Ga_{.73}As$ single-junction solar cells were grown while varying the composition of the 1.0 μm-thick $Ga_xIn_{1-x}P$ layer at the top of the graded buffer. The compositions of the eight 0.25 μm-thick intermediate steps of the grade were spaced linearly from $Ga_{.51}In_{.49}P$ to $Ga_xIn_{1-x}P$ as illustrated in Fig. 1. Fig. 6 shows the growth temperature stress calculated from *in situ* MOSS measurements and the room temperature strain calculated from *ex situ* X-ray diffraction measurements for both the $In_{.27}Ga_{.73}As$ active junction and the thick $Ga_xIn_{1-x}P$ layer at the top of the graded buffer as a function of the composition of this layer. The stress in the top buffer layer remained consistently compressive (~0.1 GPa) over the entire range of compositions used, but the stress of the $In_{.27}Ga_{.73}As$ active junction varied linearly from compressive to tensile. This buffer design therefore offers significant control over the stress of lattice-mismatched devices such as this 1.0 eV solar cell. It is important to note that the zero stress condition is not achieved by grading to the lattice constant of the final $In_{.27}Ga_{.73}As$ device, but overshooting slightly to compensate for the residual compressive stress observed in all the graded buffers. In other words, the zero stress condition is achieved when a graded buffer is designed to result in a strained in-plane lattice constant equal to the unstrained lattice constant of the active devices.

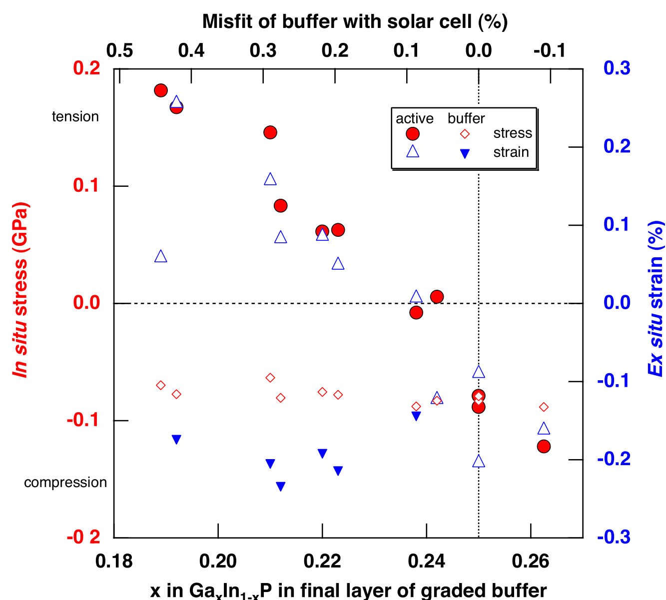

Fig. 6. Growth temperature stress calculated from *in situ* MOSS measurements and the room temperature strain calculated from *ex situ* X-ray diffraction measurements for both the $In_{.27}Ga_{.73}As$ active junction and the thick $Ga_xIn_{1-x}P$ layer at the top of the graded buffer as a function of the composition of this layer.

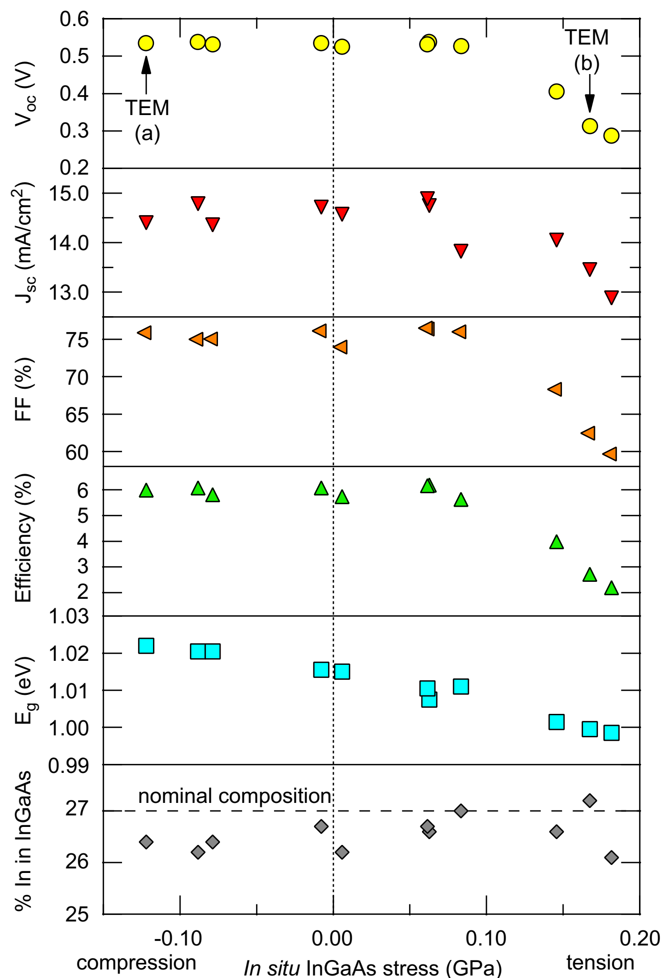

Fig. 7. Solar cell data as a function of junction stress during growth. E_g was derived from quantum efficiency data. The actual $In_xGa_{1-x}As$ composition was derived from X-ray measurements. TEM images of the indicated points are shown in Fig. 8.

The trends of the room temperature strain are in good agreement with the growth temperature stress for both layers. This is only the case because all the layers in this structure have similar thermal expansion coefficients making the contribution of Eq. (2) negligible. Growth of III–V on silicon, for example, would result in considerable change in stress/strain from growth to room temperature. The trends of the *ex situ* strain data appear to have significantly more noise than the *in situ* stress data. Some of this may be due to higher uncertainty of the X-ray strain measurement, but at least some is due to relaxation that occurs during cool-down. In particular, the sample with the highest tensile stress almost certainly has relaxed during cooldown. While not strictly correct because of different measurement conditions, the biaxial modulus can be estimated from the slope of the stress versus strain. This gives a value of about 62 GPa for the $In_{.27}Ga_{.73}As$ layer. This is comparable in magnitude at least to an interpolated value of 111 GPa from the literature [10].

The inverted $In_{.27}Ga_{.73}As$ single-junction solar cells were processed and measured as described above. The performance is plotted in Fig. 7 as a function of active layer stress. The devices grown with stress over the range of −0.05 GPa (tensile) to 0.15 GPa (compressive) had excellent performance with a open-circuit voltage (V_{oc}) of about 0.54 V. V_{oc} is typically an excellent indicator of dislocation density and the best V_{oc} that we could expect from a 1.0 eV junction is $V_{oc}{\sim}(E_g/q{-}0.4) = 0.6$ V, where q is the elementary charge. Tensile stress greater than 0.05 GPa resulted in significant device degradation. The efficiency, short-circuit current density (J_{sc}), and fill factor (FF) mirrored the trends of the V_{oc}. It should be noted, however, that the band gap of the light-filtering $Ga_xIn_{1-x}P$ buffer was varied from 1.52 to 1.57 eV in this study, artificially inflating the J_{sc} of the devices in compression relative to the devices in tension. Thus, if the devices had been optically filtered by GaAs, as in the multi-junction device, a very slight decline in the J_{sc} would have been observed as the device stress decreased from zero into compression. While we have not explored far enough, high compressive stress is also likely to result in more significant device degradation. Certainly, growth of the device without a graded buffer would result in extremely high compressive stress (1.9% misfit strain) that would relax during growth, creating many dislocations. CL revealed dislocation densities in the low 10^6 cm^{-2} for devices grown under zero stress and moderate (−0.10 GPa) compressive stress with corresponding V_{oc}'s of 0.54 V, but CL of a device under tensile stress (0.17 GPa) with a V_{oc} of 0.32 V had a dislocation density in the high 10^6 cm^{-2} range. Cross-sectional TEM images, shown in Fig. 8, confirmed the difference in dislocation densities between the compressive and tensile stressed devices, with

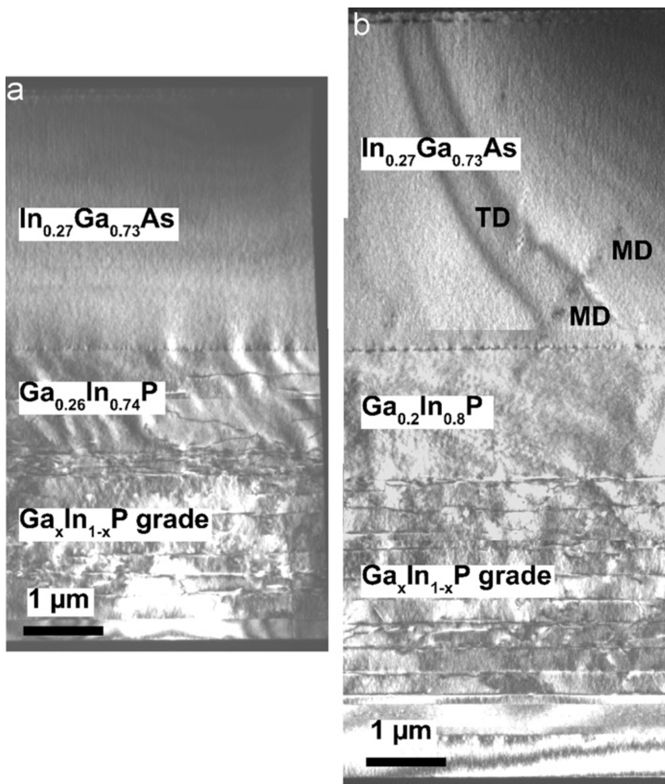

Fig. 8. The 220 dark field TEM images of two inverted InGaAs solar cells grown with different film stress in the active layer: (a) 0.12 GPa compressive and (b) 0.17 GPa tensile. Threading dislocations (TD) and the ends of misfit dislocations (MD) are observed in the thick InGaAs layer of sample *b*.

obvious threading and misfit dislocations for the device under tension and none observable in the device under moderate compression. The range of device stress that results in excellent performance is unexpectedly wide. It is possible that this window would narrow for reliability data under long-term real-life conditions such as high temperature or current operation.

Fig. 7 also shows the measured band gap and composition of the nominally $In_{.27}Ga_{.73}As$ device. Not surprisingly, the band gap of the device is systematically varied with stress while the actual composition did not vary more than the uncertainty of the measurement. The measurement and control of stress, independent of composition, using this graded buffer design may also be useful for precise control of band gap in many other opto-electronic devices as well as solar cells.

4. Conclusions

In situ stress measurements using MOSS can be very useful for optimization of lattice-mismatched devices such as solar cells. We have discussed methods to address the considerable effects of temperature on this measurement that occur in atmospheric-pressure MOVPE. We have demonstrated how the stress in devices can be controlled using a graded buffer design. The lattice-mismatched 1.0 eV $In_{.27}Ga_{.73}As$ solar cell shows excellent performance over a relatively wide range near zero stress and slightly compressive stress, but degrades more quickly under tension. This degradation is correlated with an increase in dislocation densities from the low $10^6\,cm^{-2}$ to the high $10^6\,cm^{-2}$. The MOSS measurements are a good complement to X-ray diffraction data, and could completely replace the X-ray measurements in production of lattice-mismatched devices for rapid quality control.

Acknowledgments

The authors thank C. Kramer and M. Young for dedicated work fabricating devices and M. Wanlass and S. Kurtz for the initial design of the device and helpful discussions. A. Levander thanks the DOE SULI program for financial support. This work was funded by the United States Department of Energy under contract #DE-AC36-99-GO10337.

References

[1] J.F. Geisz, S. Kurtz, M.W. Wanlass, J.S. Ward, A. Duda, D.J. Friedman, J.M. Olson, W.E. McMahon, T.E. Moriarty, J.T. Kiehl, Appl. Phys. Lett. 91 (2007) 023502.
[2] S.P. Ahrenkiel, M.W. Wanlass, J.J. Carapella, L.M. Gedvilas, B.M. Keyes, R.K. Ahrenkiel, H.R. Moutinho, J. Electron. Mater. 33 (2004) 185.
[3] J. Tersoff, Appl. Phys. Lett. 62 (1993) 693.
[4] C. Lynch, R. Beresford, E. Chason, J. Vac. Sci. Technol. B 22 (2004) 1539.
[5] R.S. Goldman, K.L. Kavanagh, H.H. Wieder, S.N. Ehrlich, R.M. Feenstra, J. Appl. Phys. 83 (1998) 5137.
[6] P. van der Sluis, J. Phys. D Appl. Phys. 26 (1993) A188.
[7] K.A. Emery, D. Myers, S. Kurtz, in: Proceedings of the 29th Photovoltaics Specialists Conference, IEEE, New Orleans, 2002, p. 840.
[8] G.G. Stoney, Proc. R. Soc. London Ser. A 182 (1909) 172.
[9] T.-C. Chen, W.-J. Lin, D.-L. Chen, J. Appl. Phys. 96 (2004) 3800.
[10] O. Madelung (Ed.), Semiconductors: Group IV Elements and III–V Compounds, Springer, Berlin, 1991.